ELSEVIER

Contents lists available at ScienceDirect

Journal of Wind Engineering & Industrial Aerodynamics

journal homepage: www.elsevier.com/locate/jweia





Performance of different inflow turbulence methods for wind engineering applications

Zahra Mansouri ^a, Rathinam Panneer Selvam ^{a,*}, Arindam Gan Chowdhury ^b

- a BELL 4190. University of Arkansas. Favetteville, AR, 72701, USA
- ^b Florida International University, Miami, FL, USA

ARTICLE INFO

Keywords: Synthetic inflow turbulence Turbulence inflow tool Large eddy simulation Digital filter method Synthetic eddy methods Divergence free synthetic eddy method Anisotropy turbulent spot method

ABSTRACT

Defining the correct inlet boundary conditions for large eddy simulations is a critical issue in computational wind engineering. Since synthetic inflow turbulence does not require costly prior flow simulations like recycling or precursor methods, it is a preferable approach. In this study, different synthetic turbulence generator methods are considered to investigate their performance in wind engineering applications. The considered methods are a) Digital Filter Methods (DFM), b) Synthetic eddy methods (SEM) with different shape functions, c) Divergence Free Synthetic Eddy Method (DFSEM), and d) two types of Anisotropy Turbulent Spot Method (ATSM). These methods are provided in Turbulence Inflow Tool (TInF) from the SimCenter (https://simcenter.designsafe-ci.org/backend-components/tinf/). Additionally, velocity spectrum at the inlet and building location is compared to the Von Karman spectrum for different inflow methods to determine how well the energy is carried from the inlet to the building location. Furthermore, different methods are evaluated to see whether they produce spurious pressure in the domain. It is concluded that spurious pressure exists in all the considered methods except SEM method with the Gaussian shape function (SEM-G). In addition, SEM-G is found to be a suitable method for peak pressure prediction on buildings with upmost 30% error.

1. Introduction

Winds are the most damaging compared to all other environmental loads on buildings and structures. Almost 75 percent of all disaster claims paid by insurance providers have resulted from tornado and hurricane damage in the last 20 years (Exponent, n.d.). Wind engineering helps to mitigate the risk of future damage by understanding the wind's mechanism. When the wind is obstructed by a structure, it applies forces to the structure. The disastrous failure of structures caused by strong winds is mainly due to the underestimation of peak wind pressures while designing the building components. Building codes provide approximate wind pressure on buildings. More precise wind pressure estimation requires field measurements, wind-tunnel testing, or computational fluid dynamics (CFD) models of wind flow. As an illustration, for component and cladding, the maximum peak pressure coefficient (Cp), obtained from ASCE 7–16, is -3.2 for a low-rise building. However, field measurements have reported that the maximum peak Cp on a low-rise building can be even lower than -8 for the Silsoe building (Richards et al., 2007).

Conducting field measurements for design purposes is expensive and

time-consuming, CFD can be an economical tool for engineers to estimate wind pressures on buildings. Furthermore, as the flow speed increases, the flow tends to be more unstable and irregular. Most flows in nature are categorized in this type of flow which is called turbulent flow. Strong winds are highly turbulent and if wind turbulence is not reasonably accounted for, the computed wind loads would not be accurate for building design purposes. Wind turbulence impacts can be incorporated using various turbulence modeling methods in CFD. Among all turbulence modeling methods, Large Eddy Simulation (LES) is economically feasible and provides an acceptable level of accuracy for peak pressure estimation.

1.1. Inflow turbulence generation methods

LES simulations without an inflow turbulence field results in underestimation of peak pressure coefficients. As a result, a proper turbulent flow field at the inlet as an inflow boundary condition (BC) is required to predict peak Cp correctly. The turbulent flow field's behavior in the interior domain is extremely dependent on the inflow field's physical quality. Thus, a critical aspect of the numerical LES is

E-mail addresses: zmansour@uark.edu (Z. Mansouri), rps@uark.edu (R.P. Selvam), chowdhur@fiu.edu (A.G. Chowdhury).

^{*} Corresponding author.

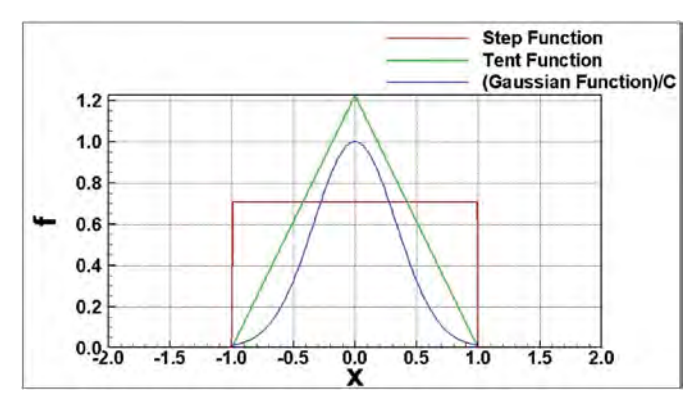


Fig. 1. Different SEM method shape functions.

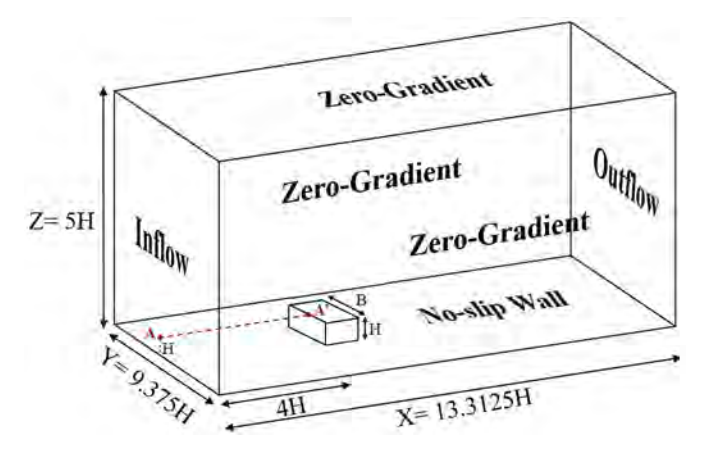


Fig. 2. Boundary conditions for the numerical modeling.

Table 1
Turbulent characteristics for the TTU building (Aboshosha et al., 2015; Mooneghi et al., 2016).

Test Characteristics	WT 1:6 Model
Integral length scale	$L_{11} = 0.43m, L_{12} = 0.2m$ and $L_{13} = 0.13$ m
	$L_{21} = 0.2L_{11} = L_{22} = L_{23}$
	$L_{31} = 0.3L_{11} = L_{32} = L_{33}$
Reference height	H=0.66m
Reference wind velocity	$U_H = 19.48 \ m/s$
Mean velocity	$U_{ave} = U_H \left(\frac{z}{H}\right)^{\alpha} m/s, \ \alpha = 0.326$
Turbulent lengh scale L	$L_j = L_{1j} \left(\frac{z}{H}\right)^{dj} m$
	$L_{11} = 0.43, L_{12} = 0.2$ and $L_{13} = 0.13$ m
	dj = 0.473, 0.881, 1.539 in the u, v and w directions
Reynolds stresses	$R_{11} = 4.3 R_{12} = 1.8$
	$R_{22} = 3.6 R_{23} = 1.8$
	$R_{33} = 3.5 R_{13} = 1.8$
Eddy density	1 only for SEM and DFSEM
Grid factor	1 only for DFM
Filter factor	4 only for DFM

defining the right inflow turbulence BC as mentioned by Selvam (1997). Selvam (1997) reported at least 30% error in CFD peak Cp compared to field measurements which was due to low grid resolution and inflow BCs. Thornber et al. (2010) reported that although very fine grid is needed to capture an appropriately broad range of initial scales, mixing layer growth is strongly dependent on initial boundary conditions. Enormous inflow turbulence generation methods are developed which are primarily categorized to (a) precursor database, (b) recycling method, and (c) synthetic turbulence (Keating et al., 2004). The

weakness of the first and second methods is the need for a database that makes these methods computationally expensive. As synthetic inflow turbulence does not require costly prior flow simulations, it is a more economically practical approach (Aboshosha et al., 2015; Ding et al., 2019). Synthetic turbulence methods include a wide range of methods that can be classified into a) Random Flow Generation Methods (RFG), b) Digital filter methods (DFM), and c) Synthetic Eddy Method (SEM). In following, a summary of the basics of each method is provided.

DFM filters a random velocity field to produce spatial and temporal coherent structures. This method does not satisfy the divergence-free condition and produces unphysically large pressure fluctuations in LES. Hence, Kim et al. (2013) first used a simple correction to maintain the constant mass flux in the inflow field, and then, inserted the generated turbulence inflow to the plane near the inlet during the procedure which led to velocities being adjusted by the velocity-pressure coupling procedure.

The idea of SEM, initiated by Jarrin et al. (2006), is rooted in the reproducing boundary layer using direct superposition of the representative coherent eddy structures. SEM assumes the flow contains randomly distributed turbulent spots. Every turbulent spot is modeled by a three-dimensional suitably normalized shape function with a compact support. Shape function depends on the two-point autocorrelation function and the power spectrum of the synthetic turbulence. In this study, for SEM, three different shape functions, i.e., Gaussian (SEM-G), Tent (SEM-T), and Step (SEM-S), are considered. For $0 \le |x| < 1$, the equation of Tent shape function (Jarrin et al., 2009) is $f = \sqrt{3/2}(1-|x|)$, for Step Shape function (Jarrin, 2008), it is $f = \sqrt{1/2}$, and for Gaussian Shape function (Jarrin, 2008), it is $f = Ce^{-9x^2/2}$,

where C is a constant that satisfies $\int_{-1}^{1} f^2(x) dx = 1$. For $|x| \ge 1$, the amount of f is zero for all shape functions. In Fig. 1, you can see the diagram for each shape function.

However, SEM like DFM is not divergence-free. Hence, Poletto et al. (2013) obtained a divergence-free method by applying SEM to the vorticity field and taking the curl of it to change back to the velocity field, i.e., Divergence Free Synthetic Eddy Method (DFSEM). Later, Kröger and Kornev (2018) proposed the Anisotropy Turbulent Spot Method (ATSM) method based on the superposition of vortical structures. This led to having explicit control on the three turbulence intensities and three integral length scales. The TInF tool refers Klein et al. (2003) and Xie and Castro (2008) for DFM, Jarrin et al. (2006) for SEM, Poletto et al. (2013) for and Kröger and Kornev (2018) for ATSM as the source of the program they used in the OpenFOAM. The performance of these inflow turbulence methods is evaluated in this paper.

Nowadays, cutting-edge improvements in computational resources led to using higher grid resolution and the development of computational simulations with a promise of becoming adaptable, accessible, and reliable means for wind load estimations (Ding et al., 2019). However, there is not a proper evaluation of the characteristics and applicability of different synthetic inflow methods from the perspective of wind engineering. Hence, in this study, to evaluate different methods' performances for the wind engineering application, DFM, SEM with three different shape functions, DFSEM, and two types of ATSM are considered.

In the ATSM-R method Reynolds stresses are provided as input and only the two length scales (L_{11} and L_{22}) are taken from the input and the third one (L_{33}) is calculated internally from a constraint equation reported in Kröger and Kornev (2018). Similarly, in the ATSM-L method all the three length scales are given as input and the modified Reynolds stresses are calculated from minimization principle. The details of the derivations and the final equations are detailed in Kröger and Kornev (2018).

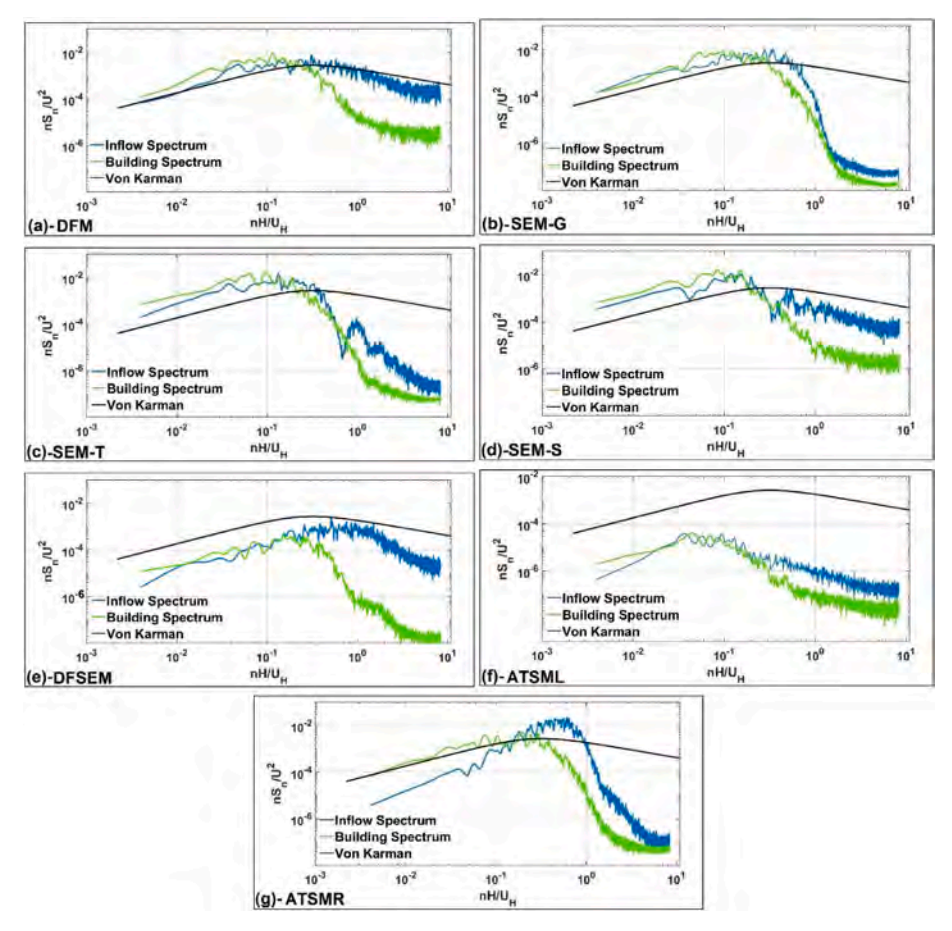


Fig. 3. Spectrum plot at the inlet and building location for a) DFM, b) SEM-G (i.e with guassian shape function), c) SEM-T (i.e with tent shape function), d) SEM-S (i.e with step shape function), e) DFSEM with eddy density = 1, f) ATSML, and g)ATSMR model for dx=H/8 and dt=0.002s (i.e. 0.03 units.

1.2. Velocity spectrum at the inlet and building location

Turbulent flow includes some circular movement of fluid called eddies. As turbulence is three-dimensional (3D) and unsteady with a large range of eddies that need to be resolved, it is necessary to develop the inflow velocity fields suitable for different scale features. In a typical turbulent flow, there exists a wide range of eddy sizes fluctuating at different frequencies (i.e., large eddies have large velocity fluctuations of low frequency and vice versa). The wind velocity spectrum describes the frequency distribution of turbulent wind flow and shows which range of eddies are produced by the inflow method. Hence, firstly, the velocity spectrum produced by the inflow method should be comparable to the Von Karman spectrum which describes the frequency distribution of the real turbulent wind flow. Furthermore, to have more accurate numerical results, the energy should not be dissipated in the building location compared to the inlet location. Rana et al. (2011) reported that DFM turbulent inflow data dissipates immediately in the computational domain because the energy is not distributed over the required range of frequencies. To reduce the numerical dissipation of the scheme and thus improve the accuracy of the results, Kokkinos's et al. (2020) tried to budget energy to low-frequency, particularly for under-resolved grids. Mansouri et al. (2022) stated that the maximum frequency as an input for the inflow methods should be determined using the largest grid spacing size in the computational domain to have a similar velocity spectrum at the inlet and building location. In this study, DFM, SEM with three shape functions, DFSEM, and two types of ATSM are considered. The inputs to these methods are Reynolds stresses and length scales, therefore, maximum and minimum frequency cannot be predetermined as inputs. Hence, the maximum frequency of inlet velocity spectrum produced by these methods is regardless of the grid spacing size.

Consequently, it is not clear how well the inlet and building location velocity spectrums are similar.

1.3. Spurious pressure due to high frequency

As mentioned above, Mansouri et al. (2022) reported the largest grid spacing (h) in the computational domain determines the highest frequency of the velocity fluctuations that can be transported by the grid. For a specific grid spacing of h, the theoretical wavelength (L) of a wave in the form of sine or cosine function transported by a spectral method is 2h (Orszag, 1979). The corresponding frequency is called Nyquist frequency in the spectral analysis. Even though transport of Nyquist frequency is possible with the spectral method, the amount of error using the finite difference method (FDM) is significant. Hence, the smallest wavelength resolved by a grid is $\lambda_{grid} = 4h$ (Mansouri et al., 2022). Hence, the maximum non-dimensional frequency transported in the flow using the finite difference method (FDM) is calculated as $f_{grid} = H/4h$ using Eqn. (1). The high frequencies beyond this value are modeled by subgrid-scale modeling like the Smograinsky model (Mansouri et al., 2022).

$$f = \frac{H}{\lambda} = \frac{nH}{U_H} \tag{1}$$

Where n is dimensional frequency, λ is the wavelength, H is the height of the building, and U_H is the mean velocity at the building height. Mansouri et al. (2022) reported that if $f_{max} > f_{grid}$, then there are spurious pressures (f_{max} is the maximum frequency as the input to the inflow method). Spurious pressures happen when the frequency of pressure goes beyond Nyquist frequency (Mansouri et al., 2022). They showed

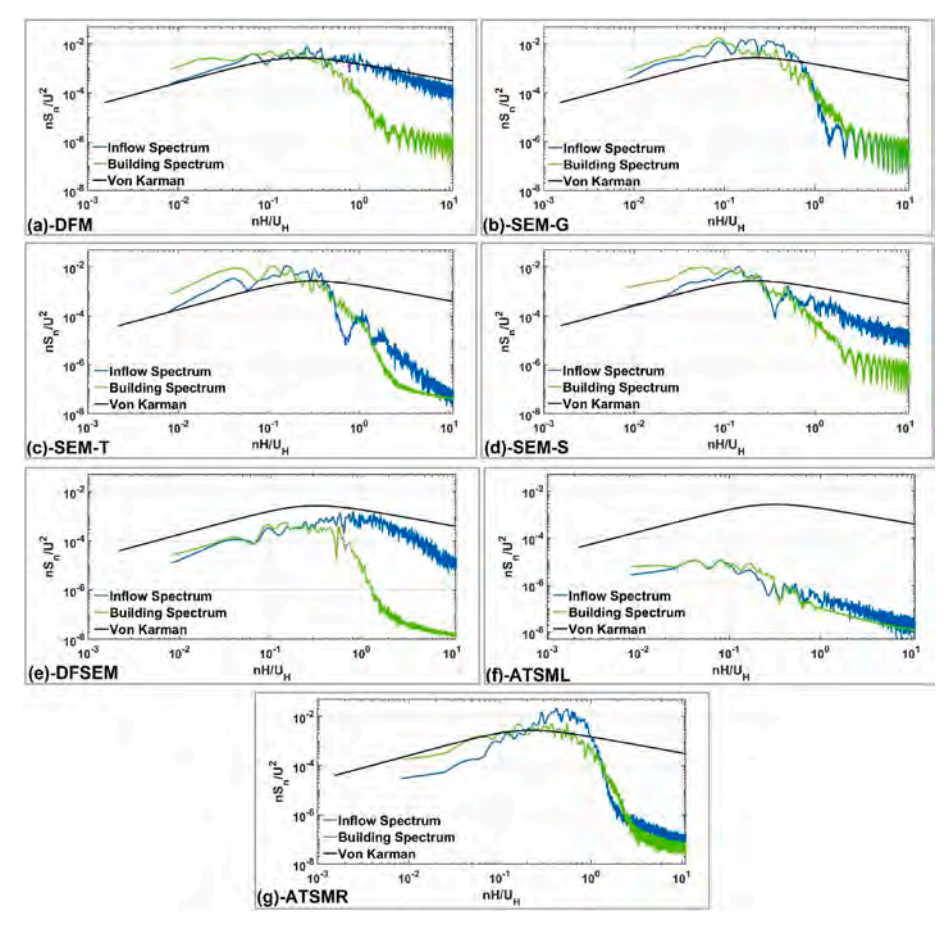


Fig. 4. Spectrum plot at the inlet and building location for a) DFM, b) SEM-G (i. e with guassian shape function), c) SEM-T (i.e with tent shape function), d) SEM-S (i. e with step shape function),e) DFSEM, f) ATSML, and g)ATSMR model for dx=H/16 and dt=0.001s (i.e. 0.01 units).

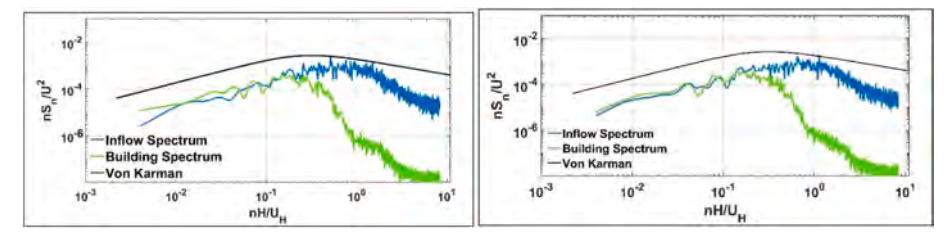


Fig. 5. Spectrum plot at the inlet and building location for DFSEM model with the eddy density of a) eddy density = 1, b) eddy density = 1000 for dx=H/8 and dt=0.002s (i.e. 0.03 units).

that the building peak pressure had high errors due to spurious pressure. It should be noted that previous researchers identified pressure fluctuation and stated some reasons for these unwanted pressures. For instance, if an inflow does not respect the Taylor hypothesis or not being divergence-free, produces unwanted pressure fluctuations (Patruno and Ricci, 2017). In addition to mentioned reasons, boundary condition mismatches leads to unwanted pressure productions near boundaries as explained in detail by Patruno and Ricci (2018). Patruno and Miranda (2020) developed a method to mitigate unwanted pressures created due to violation of divergence free condition and Taylor hypothesis. However, they used only a sinewave that respects maximum grid frequency and they stated pressure fluctuation decreases after a distance from the inlet. Whereas, Mansouri et al. (2022) indicated that pressure amplitude declined and the pressure frequency remained unchanged over the space. As here, spurious pressure was introduced based on the pressure frequency but not its amplitude, no one has evaluated inflow methods to see whether they produce spurious pressure. This study investigates

spurious pressure production.

1.4. Objectives to investigate different inflow generation method performance

In this study, DFM, SEM with three shape functions, DFSEM, and two types of ATSM method are considered. These methods are provided in the Turbulence Inflow (TInF) tool from the SimCenter (Mackenzie-Helnwein et al., 2020). Reynolds stresses and length scales inputs are prepared based on the information provided by Mooneghi et al. (2016) for the WT data of Texas Tech University (TTU) building. The major objective of this work is to evaluate the performance of different inflow turbulence generators for wind engineering applications. The criteria used to evaluate the inflow methods' performance are:

a) Comparing the velocity spectrum at the inlet location and building location with the Von Karman spectrum for two different grid

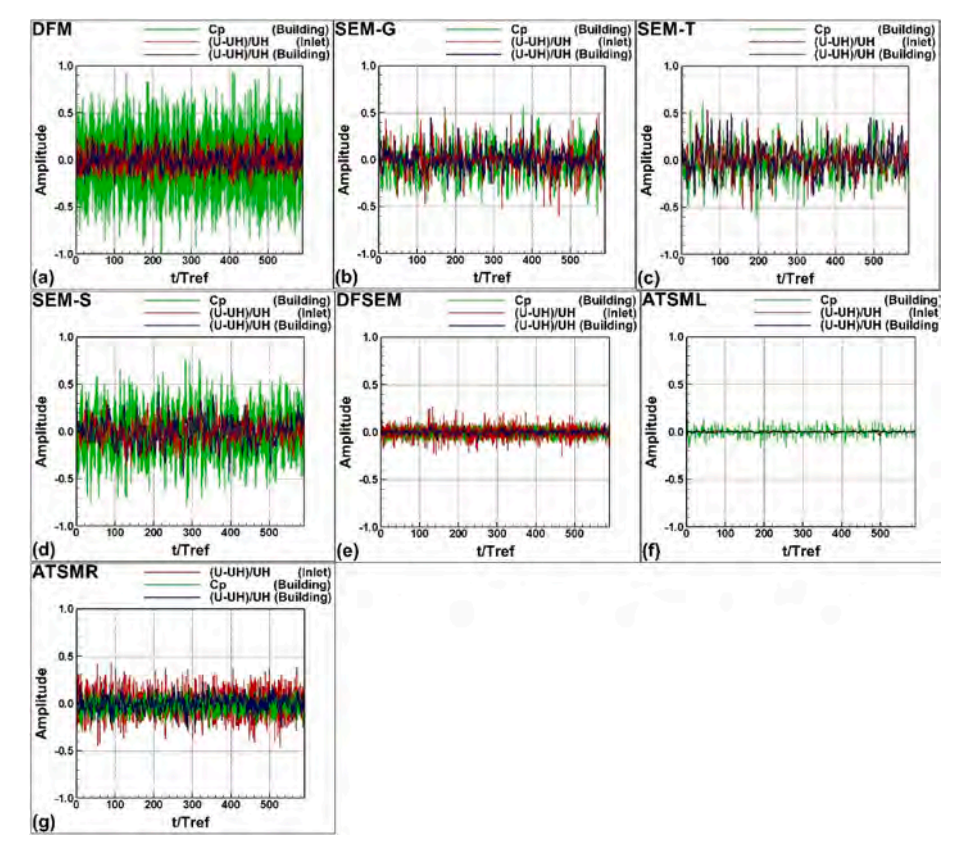


Fig. 6. Nondimensional velocity at the inlet and building location and Cp at the building location for a) DFM, b) SEM-G (i.e with guassian shape function), c) SEM-T (i.e with tent shape function), d) SEM-S (i.e with step shape function),e) DFSEM, f) ATSML, and g)ATSMR model for dx=H/8 and dt=0.002s (i.e. 0.03 units).

- spacing sizes. This determines how well the energy is carried from the inlet location to the building location.
- b) Plotting the pressure overtime at the inlet and building location to see how much spurious pressure is produced by various inflow methods.
- c) Finally, the flow with the building is modeled for the proper inflow methods and the resulted peak pressure is compared to WT measurements reported by Moravej (2018) to compare the most proper inflow methods' performance in predicting peak pressures.

2. Numerical setup

2.1. Computer modeling and boundary conditions

In this study, the CFD program OpenFOAM is used to model flow in the domain. The 3D incompressible Navier–Stokes (NS) equations are used for flow computations, and Large Eddy Simulation (LES) with the sub-grid scale of wall-adapting local eddy viscosity model (WALE) explained by Nicoud and Ducros (1999) is used for turbulence modeling. The generalized geometric-algebraic multi-grid (GAMG) solver with a tolerance of 1e-5 is used for the pressure, and the symmetric Gauss-Seidel solver with a tolerance of 1e-6 is used for the rest of the variables. For coupling velocity and pressure, the PISO method is used, and the algorithm solves two times the pressure equation and momentum corrector in each step.

In this study, two uniform grid spacing sizes of H/8 and H/16 (where H is the building height of the Texas Tech University (TTU) building) in all directions are considered. The grid is made using "BlockMesh" generator in the OpenFOAM. More details for grid generation using "BlockMesh" are provided in Mansouri et al. (2021), Verma et al. (2021), and Selvam (2022). The dimension of the TTU building is $2.25H \times 3.375H \times H$, where H is 0.66 m. The flow is considered to be

along with the shorter length (2.25H) of the TTU building. The domain size used for computation is $13.3H \times 9.375H \times 5H$, and the building is located 4H from inflow in the computational domain as shown in Fig. 2. The grid size equals $107 \times 76 \times 41$ with 333,412 nodes for the grid spacing size of H/8 and the grid size equals $213 \times 151 \times 81$ with 2,605,203 nodes for H/16. First, the flow is modeled in the domain without building in this study, and then the flow is modeled in the domain with building for the most proper inflow method for wind engineering application. Results are provided at the inlet and building location.

The CFL (Courant–Friedrichs–Lewy) criterion is kept at less than 1.0 to capture all the time-variant issues. The maximum velocity around the building is approximately $2{\rm U_H}$ based on the computation; hence, the dimensional time step (dt) should be less than ${\rm dt}=dX/U_{max}=(H/8)/2U_H=0.0021$ to preserve CFL < 1.0 ($U_H=19.48~m/s$). In this study, a dimensional time step of dt=0.002 is used for the grid spacing size of H/8. Similarly, to preserve CFL < 1.0, a dimensional time step of dt=0.001 is used for the grid spacing size of H/16. The computation is conducted for 20 s or 590 non-dimensional time units. The computer time for the grid space of H/8 is about 4 h and for H/16 is near 3 days.

The boundary conditions are indicated for all surfaces in Fig. 2. The zero-gradient boundary conditions are implemented on the sidewalls, and the outflow boundary condition is specified at the outlet. The no-slip wall is implemented on the ground. At the inlet, the inflow turbulence is introduced. The inflow turbulence is calculated using the Turbulence Inflow (TInF) tool, which is explained in the next section. TInF tool from the SimCenter developed by Mackenzie-Helnwein et al. (2020) provided different inflow methods considered in this study.

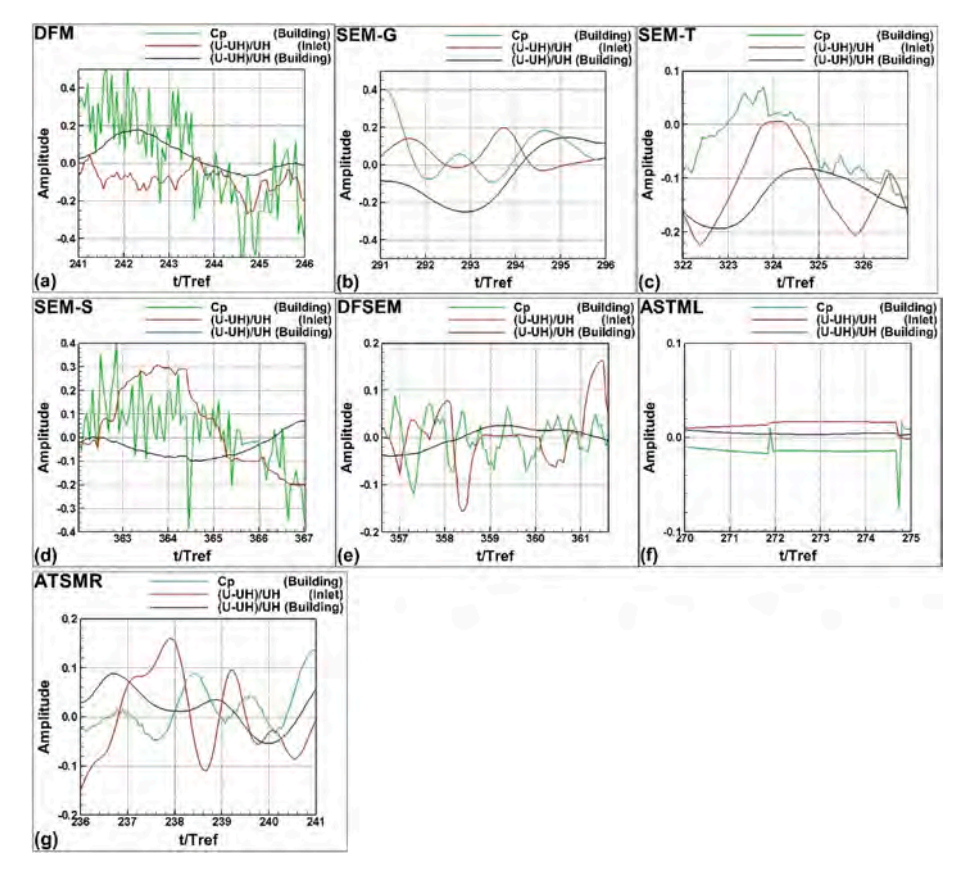


Fig. 7. Close up of nondimensional velocity at the inlet and building location and Cp at the building location for 5 time units for a) DFM, b) SEM-G (i.e with gaussian shape function), c) SEM-T (i.e with tent shape function), d) SEM-S (i.e with step shape function),e) DFSEM, f) ATSML, and g)ATSMR model for dx=H/8 and dt=0.002s (i.e. 0.03 units).

2.2. Initial condition in TInF

After mesh generation, defining boundary conditions, and modifying all OpenFOAM case files (i.e., '0', 'constant', and 'system'), TInF is used to remodify files to apply a specific inflow turbulence generation method. The information provided in Table 1 is required to use TInF tool. For using TInF tool, after choosing the inflow method, the parameters related to inlet velocity profile, length scales, and Reynolds stresses should be inserted for the inlet boundary condition as explained in Appendix A.

It should be noted that the length scales should be checked in the 'inflowProperties' file created by TInF tool in the 'constant' folder before running the case file. The length scale, L, should be defined in 'inflow-Properties' file with a nine-component $(L_{11}, L_{12}, L_{13}, L_{21}, L_{22}, L_{23}, L_{31}, L_{32}, L_{33})$ for DFM and SEM, a three-component vector of the form (L_{11}, L_{22}, L_{33}) for the ATSM boundary condition, and one component scalar (L_{11}) for the DFSEM.

The eddy density is a parameter to be given as input for SEM and DFSEM as reported in Table 1. Jarrin et al. (2009) and Poletto et al. (2013) defines eddy density 'd' as the volume of eddies in a box divided by the volume of the box. The volume of eddies is calculated as the number of eddies multiplied by the volume of an eddy. They recommend d=1 as the reasonable value and the TInF tool considers d=1 as the default value also. In the paper, we investigated further with d=1000 in section 3.2.

In case file preparation for the DFM method, the one correlation function (i.e., Gaussian, exponential or bessel) should be chosen. The details are provided in TInF tool report, section 10.2.1 (Wan and Mackenzie-Helnwein, 2020). In this study, the recommended function, i. e., exponential, is used. For exponential correlation function, it needs to provide values for grid factor and filter factor variables. In this study, the

default value of 1 and 4 are used for grid factor and filter factor respectively.

3. Results and discussion

Flow is modeled numerically for 590 nondimensional time units using different inflow turbulence generators as inflow for two grid spacing sizes of H/16 and H/8. The velocity spectrum at the inlet and building location (at the building height, which these points are shown in Fig. 2 as A(0,4.6875H,H) and A'(4H,4.6875H,H)) are plotted for 10000 time steps (i.e., about 300 nondimensional time units) using the modified MATLAB code provided by Moravej and Chowdhury (2018). To show the capability of each method in real wind turbulence field production and to determine how well the energy is carried from the inlet location to the building location, the velocity spectrum at the inlet and building location is compared to the Von Karman spectrum for different inflow turbulence fields. The velocity and pressure coefficients are plotted over time for different cases to investigate spurious pressure production and subsequently evaluate the performance of each inflow turbulence generation method. Finally, the flow with the building is modeled for the proper inflow methods and the resulted peak pressure is compared to WT measurements reported by Moravej (2018) to compare the most proper inflow methods' performance in predicting peak pressures on buildings.

3.1. Velocity spectrum at the inlet and building location for different inflow methods

The velocity spectrum is plotted for different inflow methods in Fig. 3 for the grid spacing size of H/8. According to Fig. 3. (a), the DFM method wind spectrum is comparable to the Von Karman spectrum at the inlet

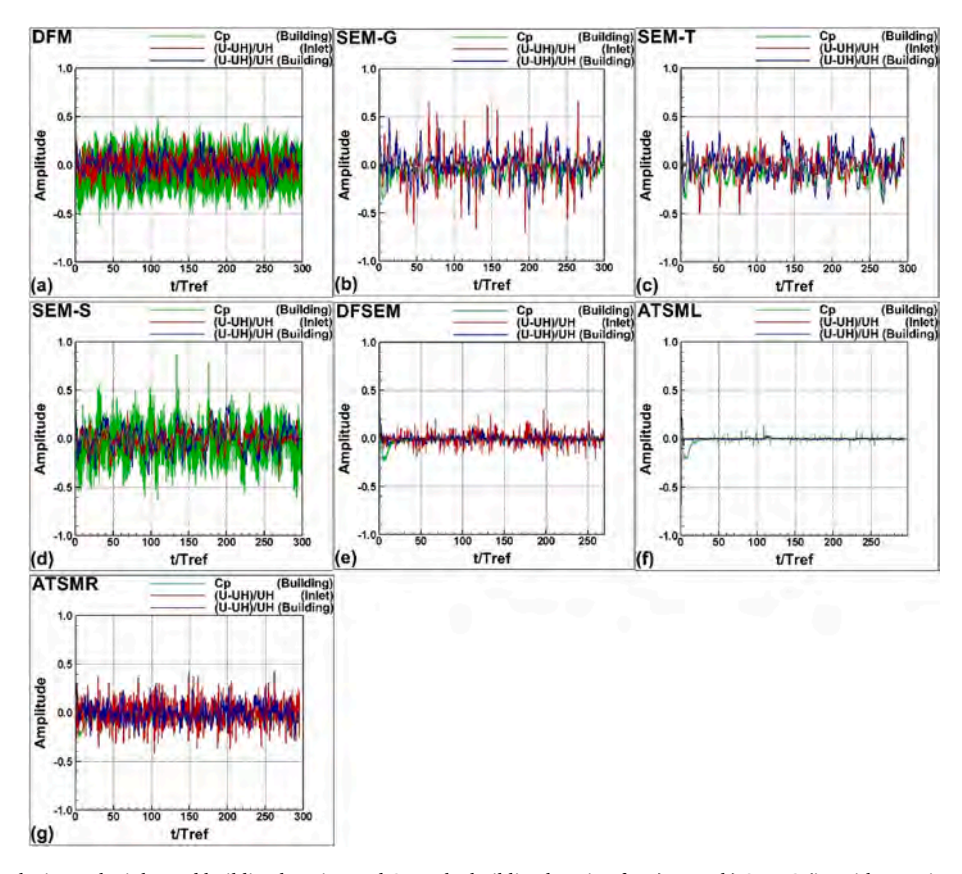


Fig. 8. Nondimensional velocity at the inlet and building location and Cp at the building location for a) DFM, b) SEM-G (i.e with guassian shape function), c) SEM-T (i.e with tent shape function), d) SEM-S (i.e with step shape function),e) DFSEM, f) ATSML, and g)ATSMR model for dx=H/16 and dt=0.001s (i.e. 0.01 units).

location for the frequency range of (0.004–9) and has a sharp decline in energy beyond f=0.2 at the building location. The SEM-G method wind spectrum is comparable to the Von Karman spectrum at the inlet location for the frequency range of (0.004–0.4) and has a sharp decline in energy beyond f=0.2 at the building location from Fig. 3. (b). This method has the most similar spectrum at the inlet and building locations.

From Fig. 3. (c) and (d), The SEM-T and SEM-S methods produced the amplitude slightly more than the Von Karman spectrum for the frequency range of (0.004–0.2). In the frequency range of (0.004–0.2), The SEM-T and SEM-S methods have approximately similar velocity spectrums at the inlet and building locations. The DFSEM and ATSML methods produce lower amplitudes of velocity spectrum compared to the Von Karman spectrum from Fig. 3 (e) and (f). According to Fig. 3. (g), the ATSMR method velocity spectrum has a higher amplitude in the low frequencies part compared to the Von Karman spectrum and vice versa.

According to Fig. 3, the SEM-G method produced the most comparable velocity spectrum at the inlet and building location. All of the considered methods produced frequency lower than the f_{grid} . The maximum frequency carried by the grid of H/8 is 2, whereas, all methods have a sharp decline in energy around f=0.2 from Fig. 3. In fact, most methods do not have much energy in the frequency range of (0.2-2).

Similarly, the velocity spectrum is plotted for different inflow methods for the grid spacing size of H/16 in Fig. 4. According to Fig. 4. (a), the DFM method inlet velocity spectrum is comparable to the Von Karman spectrum in the range of frequency of (0.008–11). Furthermore, the DFM velocity spectrum at the building location has a sharp decline in

energy at about f=0.3. The DFM method produces a greater range of high frequencies turbulences for the grid spacing of H/16 compared to the grid spacing of H/8. The SEM-G method's wind spectrum is comparable to the Von Karman spectrum at the inlet location for the frequency range of (0.008-0.7) approximately and has a sharp decline in energy beyond f=0.35 at the building location from Fig. 4. (b).

From Fig. 4. (c) and (d), the SEM-T and SEM-S methods produced the amplitude slightly more than the Von Karman spectrum for the frequency range of (0.008–0.2). Similarly, the DFSEM and ATSML methods produce lower amplitudes of velocity spectrum compared to the Von Karman spectrum for the grid spacing size of H/16 according to Fig. 4 (e) and (f). From Fig. 4. (g), the ATSMR method velocity spectrum has higher amplitude in low frequencies compared to the Von Karman spectrum and vice versa. However, the ATSMR velocity spectrum at the building location is comparable to the Von Karman spectrum in the frequency range of (0.008–0.7) and approximately has a sharp decline in energy beyond f=0.7 at the building location.

According to Fig. 4, the SEM-G method produced the most comparable velocity spectrum at the inlet and building location. The maximum frequency carried by the grid of H/16 is 4. However, all the considered methods produced frequency lower than the f_{grid} . The energy loss may be due to having high frequency components greater than f_{grid} at the inlet, violation of divergence free condition, numerical error in using FDM, and energy cascade. During the pressure correction step, the high frequency components are eliminated to get a continuous velocity and pressure at each time step and this changes the energy spectrum. Also, the energy cascade happens because none of the inflow methods satisfy the NS equation or momentum equation and this is an important factor as illustrated by Sescu and Hixon (2013). Since, several factors are

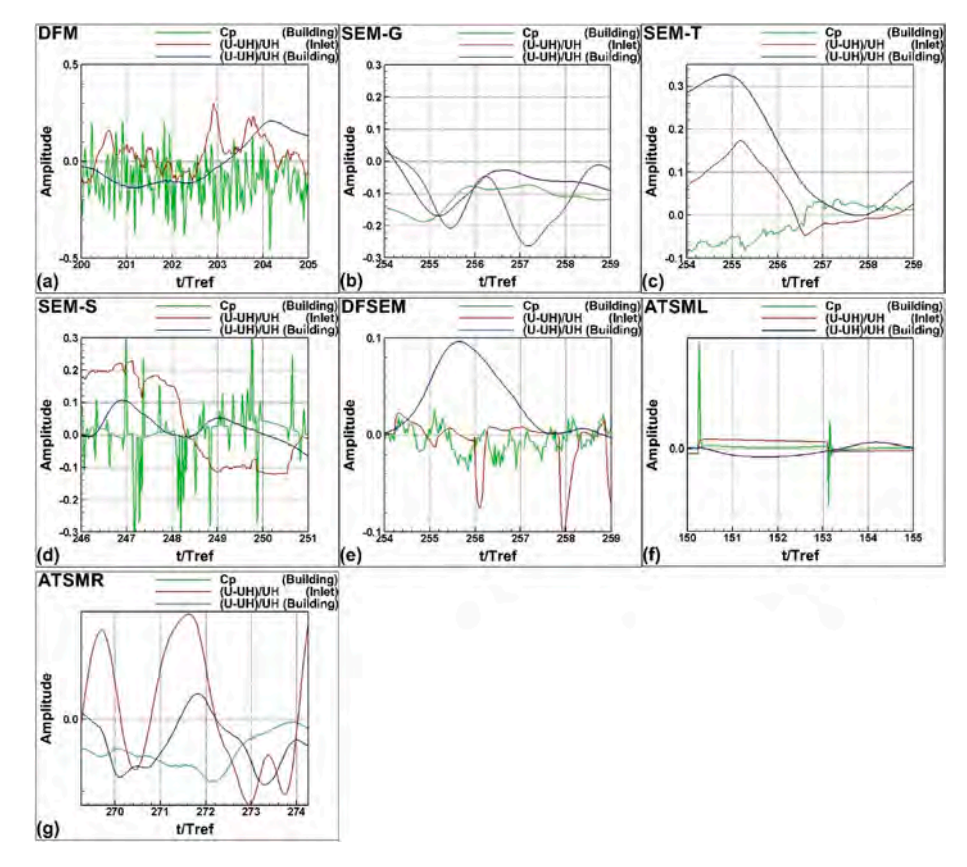


Fig. 9. Close up of nondimensional velocity at the inlet and building location and Cp at the building location for 5 time units for a) DFM, b) SEM-G (i.e with gaussian shape function), c) SEM-T (i.e with tent shape function), d) SEM-S (i.e with step shape function),e) DFSEM, f) ATSML, and g)ATSMR model for dx=H/16 and dt=0.001s (i.e. 0.01 units).

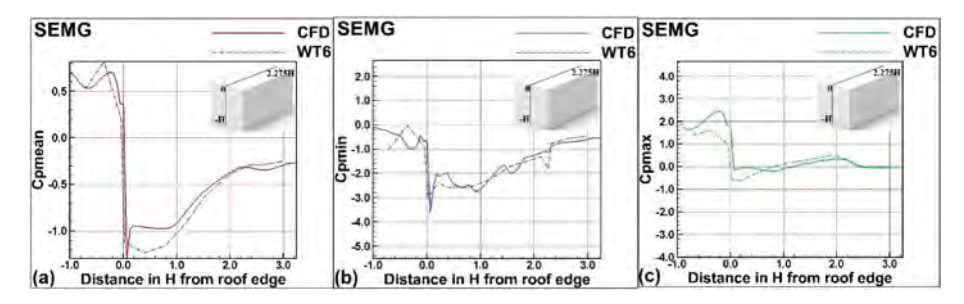


Fig. 10. CFD a) mean, b) minimum, and c) maximum pressure coefficient (*Cp*) along the centerline of the TTU building in comparison to WT measurements for the grid spacing of H/16.

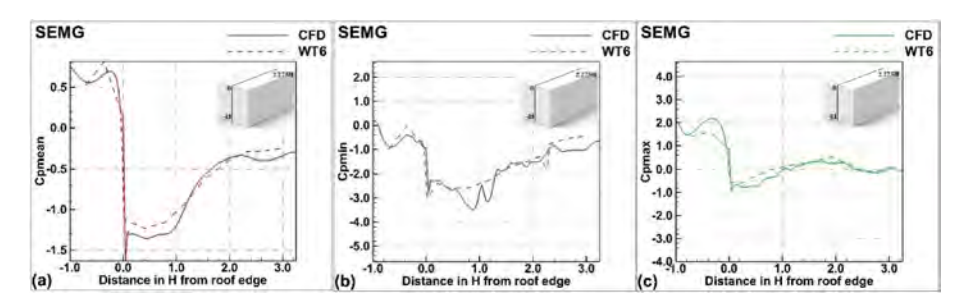


Fig. 11. CFD a) mean, b) minimum, and c) maximum pressure coefficient (*Cp*) along the centerline of the TTU building in comparison to WT measurements for the grid spacing of H/24.

involved in this issue and it is beyond the current objective, it will be investigated in the future.

3.2. The effect of eddy density on velocity spectrum

To see the effect of eddy density as input for inflow methods like SEM and DFSEM on the velocity spectrum, the velocity spectrum at the inlet and building location is plotted for two different eddy densities using DFSEM as shown in Fig. 5. In one case the amount of eddy density is considered 1 and in the other one, it is considered 1000. According to Fig. 5, eddy density does not have any considerable effect on the velocity spectrum at the inlet and building location.

3.3. Spurious pressure

To evaluate the inflow methods for spurious pressure production, the pressure coefficient is plotted at the building location. Spurious pressures happen when the frequency of pressure goes beyond Nyquist frequency. In Fig. 6, nondimensional velocity is plotted at the inlet and building location, and pressure also is plotted at the building location for different inflow turbulence fields. The grid spacing size is dx=H/8, and the time step is dt = 0.002s (i.e. 0.03 units). According to this figure, all methods have damping in the velocity amplitude at the building location compared to the amount at the inlet location. However, the amount of this deduction is significant in the DFSEM model compared to others when one looks at it closer at several places. In Fig. 7 only a particular close up for 5-time units is shown. In this figure, pressure coefficients are computed using the relation of $C_p = P/(1/2\rho U^2)$.

In Fig. 7, the close-up of velocity and pressure coefficients are plotted over 5 time units. Spurious pressure occurs when pressure frequency is higher than Nyquist frequency. For the grid spacing size of H/8, the nondimensional Nyquist frequency is H/(2h) = 8h/(2h) = 4. If frequencies are taken as the number of peaks or cycles per unit time, pressure frequencies from Fig. 7 are 8, 1, 5, 5, 6,1, and 5 for DFM, SEM-G, SEM-T, SEM-S, DFSEM, ATSML, ATSMR respectively. Hence, spurious pressures are observed in DFM, SEM-T, SEM-S, DFSEM, and ATSMR. The spurious pressure is not observed in SEM-G and ATSML. According to Figs. 3 and 7, for the SEM-G case as an example, when the wind velocity spectrum at the inlet is comparable to the building location one, then spurious pressure is not observed.

Similarly, in Fig. 8, nondimensional velocity is plotted at the inlet and building location, and pressure also is plotted at the building location for different inflow turbulence fields. The grid spacing size is dx=H/16, and the time step is dt = 0.001s. Nyquist frequency for the grid spacing size of H/16 is 8.

In Fig. 9, the close-up of velocity and pressure coefficients are plotted over 5 time units. As mentioned previously, spurious pressure happens when pressure frequency is higher than Nyquist frequency. For the grid spacing size of H/16, the nondimensional Nyquist frequency is H/(2h) = 16h/(2h) = 8. According to Fig. 9, when pressure frequencies are taken as the number of peaks per unit time, pressure frequencies are 10, 1, 9, 9, 11,1, and 10 for DFM, SEM-G, SEM-T, SEM-S, DFSEM, ATSML, ATSMR respectively. Hence, spurious pressures are observed in DFM, SEM-T, SEM-S, DFSEM, and ATSMR. Similarly, the spurious pressure is not observed in SEM-G and ATSML.

3.4. SEM-G for wind engineering application

As, ATSML is not able to produce a comparable inlet velocity spectrum to the Von Karman spectrum, ATSML cannot be employed for the Wind Engineering Application. Among considered methods, SEM-G does

not produce spurious pressure. Furthermore, the SEM-G method produced a similar velocity spectrum at the inlet and building location, which is comparable to the Von Karman spectrum. To evaluate whether SEM-G is proper for wind engineering applications, the flow around the TTU building is modeled. The CFD peak and mean pressure coefficient (*Cp*) along the centerline of the TTU building are calculated and compared to the WT measurements reported by Moravej (2018). To calculate the peak pressure, the following procedure is used. Generally, about 10 time units are needed for the turbulent flow to be fully developed, and hence it is ignored. The remaining data from 10 time units to 100 time units are considered to capture the peak pressures at each point in time. In Fig. 10 and Fig. 11, the CFD mean *Cp*, maximum *Cp* (*Cpmax*), and minimum *Cp* (*Cpmin*) are compared to WT scale 1:6 (WT6).

According to Fig. 10(a), the mean *Cp* error compared to WT6 is 30% at windward, 18% at the roof, and 24% at leeward. Corresponding to Fig. 10(b), the minimum CFD Cp error compared to WT6 is 30% at windward, 16% at the roof, and 20% at leeward. From Fig. 10(c), the maximum CFD *Cp* error compared to WT6 is 100% at windward, 40% at the roof. On the leeward side, the WT6 and CFD are approximately close together. Hence, considering at least 30% error in peak pressure estimation, SEM-G can be used in wind engineering applications.

4. Conclusion

Flow is modeled numerically for 590 nondimensional time units using different synthetic turbulence generator methods, which are provided in the Turbulence Inflow (TInF) Tool. The considered methods are a) Digital Filter Methods (DFM), b) Synthetic eddy methods (SEM), c) Divergence Free Synthetic Eddy Method (DFSEM), and d) Anisotropy Turbulent Spot Method (ATSM). The resulted velocity, pressure coefficients, and velocity spectrum overtime at the inlet and building location (at the building height) are plotted for different cases and observed:

- 1. In FDM, the maximum frequency carried by the grid is 2 and 4 for grid spacing sizes of H/8 and H/16 respectively, whereas, all methods have a sharp decline in energy as observed in Figs. 3 and 4 when the frequency is less than f_{grid} .
- 2. When the pressure frequency is higher than the Nyquist frequency of the grid, then we say there is spurious pressure. In most methods, spurious pressures are observed except in SEM-G and ATSML as shown in Figs. 7 and 9. So other methods are eliminated for wind engineering application.
- 3. Out of SEM-G and ATSML methods that have less spurious pressure at the building location, the SEM-G wind spectrum at the inlet and at the building location is much closer to the Von Karman spectrum than ATSML wind spectrum. Hence SEM-G is preferred for wind engineering applications. Using SEM-G method, the building pressure coefficients are calculated and compared with WT measurements. The computed minimum and mean pressures have a maximum 30% error at windward side of the building compared to WT6 measurements.

CRediT authorship contribution statement

Zahra Mansouri: Software, Formal analysis, Investigation, Data curation, Writing – original draft, Writing – review & editing, Visualization. **Rathinam Panneer Selvam:** Conceptualization, Methodology, Data curation, Writing – review & editing, Supervision, Project administration, Funding acquisition. **Arindam Gan Chowdhury:** Validation,

Resources, Writing - review & editing.

Declaration of competing interest

The authors declare the following financial interests/personal relationships which may be considered as potential competing interests: Zahra Mansouri reports financial support was provided by University of Arkansas Fayetteville.

Data availability

Data will be made available on request.

Notation

Mean pressure coefficient $C_p =$ C_{pmin} Minimum pressure coefficient $C_{pmax} =$ Maximum pressure coefficient dt =Non-dimensional time step dT =Dimensional time step Non-dimensional frequency $= nH/U_H = H/L$ Maximum frequency carried by the grid $f_{grid} =$ H =**Building** height Maximum grid spacing

 $\lambda_{grid} = Smallest$ wavelength transported by grid $L_1 = Turbulence$ length scale in x direction $L_2 = Turbulence$ length scale in y direction $L_3 = Turbulence$ length scale in z direction $L_3 = Turbulence$ length scale in z direction $L_3 = Turbulence$ Dimensional frequency

 $T_{ref} = ext{Reference time}$ $U_{ave} = ext{Average velocity}$

 $U_H =$ Average velocity at building height

Appendix A. Using TInF

a. To use TInF, by pressing 'Locate', the source file including '0', 'constant', and 'system' files should be chosen. Afterward, the 'inlet' face should be chosen in the 'select what boundary to modify' which is shown in Fig.A1.

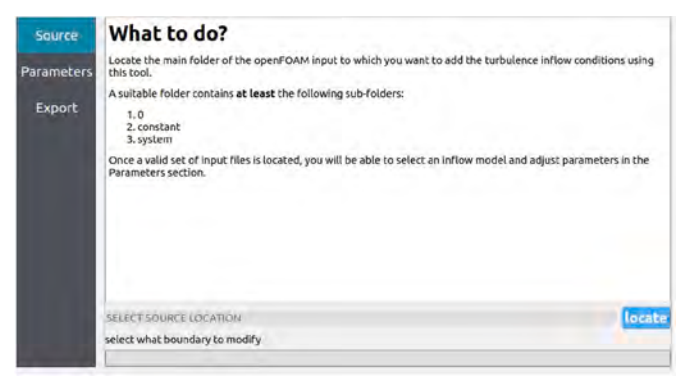
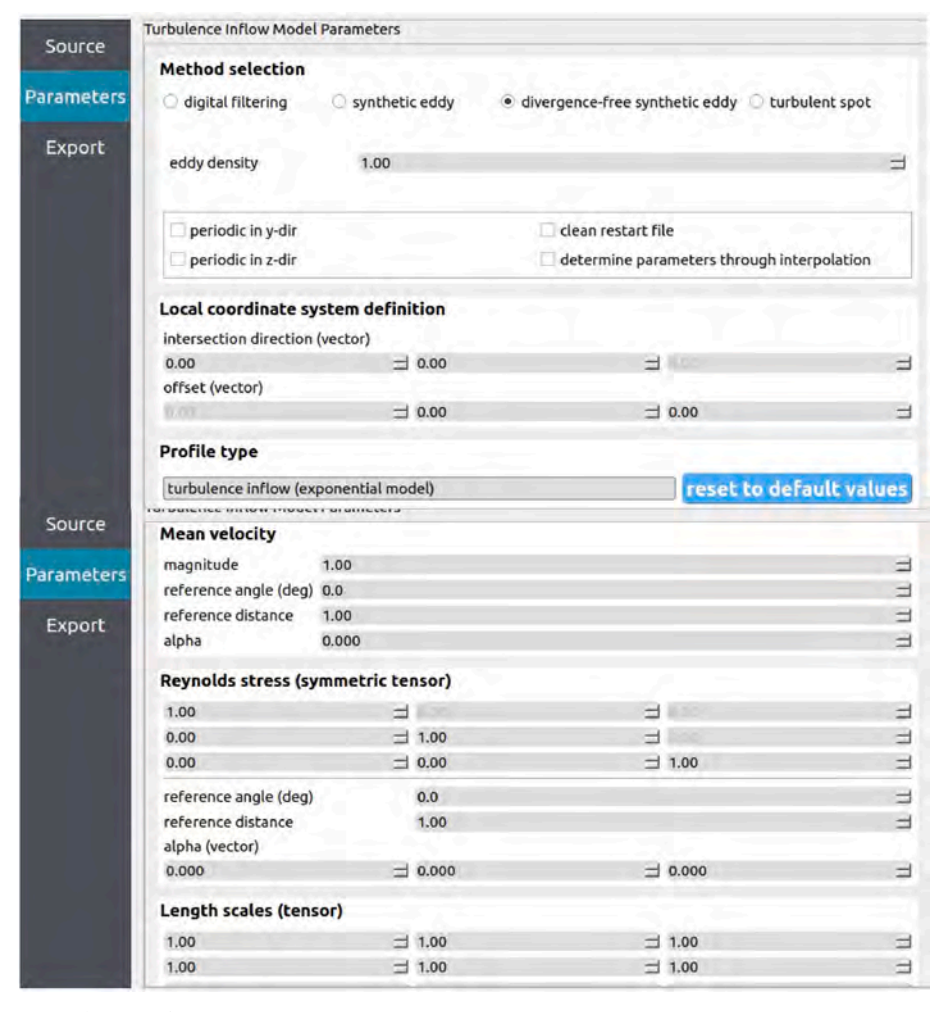


Fig. A.1. The source section of TInF tools.

b. Based on Table 1, parameters should be inserted in the parameter section, which is indicated in Fig.A2.

Acknowledgments

Ms. Zahra Mansouri acknowledges the financial support from the James T. Womble Professorship from the University of Arkansas. For this research, wind tunnel data from the NHERI WOW EF were used. The authors acknowledge the help provided by Dr. M. Moravej from Walker Consultants in delivering the wind tunnel data in a way we could use in this study. The authors acknowledge the support from Dr. P. Mackenzie-Helnwein from NEHRI SimCenter to use the TInF tool in case file preparations for OpenFOAM. The authors acknowledge unknown reviewers for the valuable comments to improve the paper.



 $\textbf{Fig. A.2.} \ \ \textbf{The parameters section of TInF tools.}$

c. Finally, the 'inlet' face should be chosen in the 'select what boundary to modify' in the 'Export' section. Then the 'Export' key should be pressed to modify files (Fig. A3.).

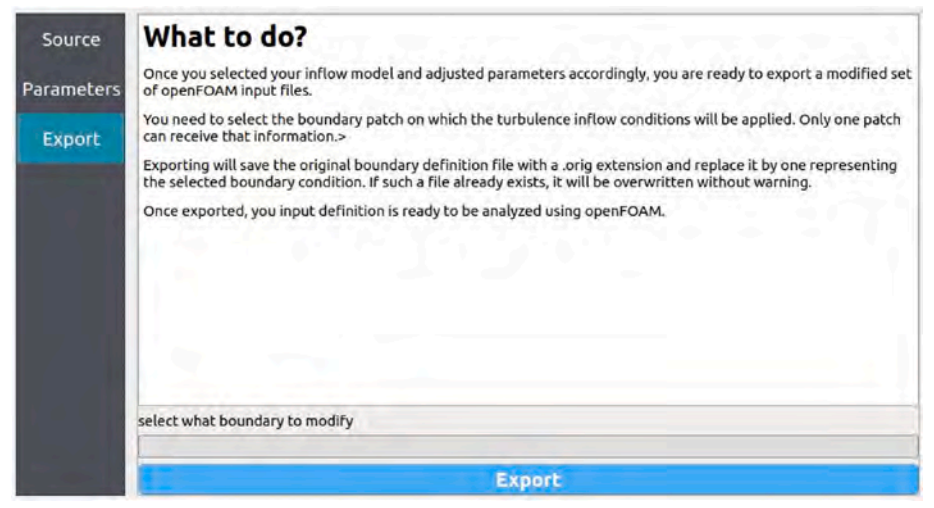


Fig. A.3. The source section of TInF tools.

References

- Aboshosha, H., Elshaer, A., Bitsuamlak, G.T., El Damatty, A., 2015. Consistent inflow turbulence generator for LES evaluation of wind-induced responses for tall buildings. J. Wind Eng. Ind. Aerod. 142, 198–216.
- Ding, F., Kareem, A., Wan, J., 2019. Aerodynamic tailoring of structures using computational fluid dynamics. Struct. Eng. Int. 29, 26–39.
- Exponent, Engineering and scientific consulting, Wind Eng., https://www.exponent.com/services/practices/engineering/buildings-structures/capabilities/wind-engineering/?serviceld=c16fc389-0037-4f90-a173-4171d47c37ad&loadAllByPageSize=true&knowledgePageSize=7&knowledgePageNum=0&noserofessionalsPageNum=0&noserofessionalsPageNum=1.
- Jarrin, N., 2008. Synthetic Inflow Boundary Conditions for the Numerical Simulation of Turbulence. Ph.D. thesis. University of Manchester.
- Jarrin, N., Benhamadouche, S., Laurence, D., Prosser, R., 2006. A Synthetic-eddy-method for generating inflow conditions for large-eddy simulations. Int. J. Heat Fluid Flow 27, 585–593.
- Jarrin, N., Revell, A., Prosser, R., Laurence, D., 2009. Reconstruction of turbulent fluctuations for hybrid RANS/LES simulations using a synthetic-eddy-method. Int. J. Heat Fluid Flow 30, 435–442.
- Keating, A., Piomelli, U., Balaras, E., Kaltenbach, H.J., 2004. A priori and a posteriori tests of inflow conditions for large-eddy simulation. Phys. Fluids 16, 4696–4712.
- Kim, Y., Castro, I.P., Xie, Z.T., 2013. Divergence-free turbulence inflow conditions for large-eddy simulations with incompressible flow solvers. Comput. Fluids 84, 56–68.
- Klein, M., Sadiki, A., Janicka, J., 2003. A digital filter based generation of inflow data for spatially developing direct numerical or large eddy simulations. J. Comput. Phys. 186 (2), 652–665.
- Kokkinakis, I.W., Drikakis, D., Ritos, K., Spottswood, S.M., 2020. Direct numerical simulation of supersonic flow and acoustics over a compression ramp. Phys. Fluids 32, 066107.
- Kröger, H., Kornev, N., 2018. Generation of divergence free synthetic inflow turbulence with arbitrary anisotropy. Comput. Fluids 165, 78–88.
- Mackenzie-Helnwein, P., Wan, J.J., McKenna, F., 2020. NHERI-SimCenter/ TurbulenceInflowTool. version 1.1.0 (v1.1.0). https://doi.org/10.5281/ zenodo.3988635. Zenodo.
- Mansouri, Z., Verma, S., Selvam, R.P., 2021. Teaching modeling turbulent flow around building using LES turbulence method and open-source software OpenFOAM. In: 2021 ASEE Midwest Section Conference.
- Mansouri, Z., Selvam, R.P., Chowdhury, A., 2022. Maximum grid spacing effect on peak pressure computation using inflow turbulence generators. Results Eng. J. in press.

- Mooneghi, M.A., Irwin, P., Chowdhury, A.G., 2016. Partial turbulence simulation method for predicting peak wind loads on small structures and building appurtenances. J. Wind Eng. Ind. Aerod. 157, 47–62.
- Moravej, M., 2018. Investigating Scale Effects on Analytical Methods of Predicting Peak Wind Loads on Buildings. Ph.D. thesis. FIU, Miami, Florida.
- Moravej, M., Chowdhury, A.G., 2018. Wind Analysis Tools: Power Spectra. DesignSafe-
- Nicoud, F., Ducros, F., 1999. Subgrid-scale stress modelling based on the square of the velocity gradient tensor. Flow, Turbul. Combust. 62, 183–200.
- Orszag, S.A., 1979. Spectral methods for problems in complex geometrics. In: Parter, S.V. (Ed.), Numerical Methods for Partial Differential Equations. Academic Press, pp. 273–305.
- Patruno, L., de Miranda, S., 2020. Unsteady inflow conditions: a variationally based solution to the insurgence of pressure fluctuations. Comput. Methods Appl. Mech. Eng. 363, 112894.
- Patruno, L., Ricci, M., 2017. On the generation of synthetic divergence-free homogeneous anisotropic turbulence. Comput. Methods Appl. Mech. Eng. 315, 396–417.
- Patruno, L., Ricci, M., 2018. A systematic approach to the generation of synthetic turbulence using spectral methods, Comput. Methods Appl. Mech. Eng. 340, 881–904
- Poletto, R., Craft, T., Revell, A., 2013. A new divergence free synthetic eddy method for the reproduction of inlet flow conditions for LES. Flow, Turbul. Combust. 91, 519–539
- Rana, Z.A., Thornber, B., Drikakis, D., 2011. On the importance of generating accurate turbulent boundary condition for unsteady simulations. J. Turbul. 12, N35.
- Richards, P.J., Hoxey, R.P., Connell, B.D., Lander, D.P., 2007. Wind-tunnel modelling of the Silsoe cube. J. Wind Eng. Ind. Aerod. 95, 1384–1399.
- Selvam, R.P., 1997. Computation of pressures on Texas Tech University building using large eddy simulation. J. Wind Eng. Ind. Aerod. 67, 647–657.
- Selvam, R., 2022. Computational Fluid Dynamics for Wind Engineering. Wiley-Blackwell, Chichester.
- Sescu, A., Hixon, A., 2013. Toward low-noise synthetic turbulent inflow conditions for aeroacoustic calculations. Int. J. Numer. Methods Fluid. 73, 1001–1010.
- Thornber, B., Drikakis, D., Youngs, D.L., Williams, R.J.R., 2010. The influence of initial conditions on turbulent mixing due to Richtmyer–Meshkov instability. J. Fluid Mech. 654, 99–139 (B).
- Verma, S., Mansouri, Z., Selvam, R.P., 2021. Incorporating two weeks open-source software lab module in CFD and fluids courses. In: 2021 ASEE Midwest Section Conference.
- Wan, J., Mackenzie-Helnwein, P., 2020, TInF Tool Release 1.1.0, Report,